AN UNSTRUCTURED REVERSE MONTE CARLO METHOD FOR SOLVING RADIATIVE INTENSITY IN GRAY MEDIA WITH COMPLEX GEOMETRIES

Jianjun LIU[1,2*], Zhiwei LI[2], Liqi ZHANG[1]

[1] State Key Laboratory of Coal Combustion, Huazhong University of Science and Technology, Wuhan, Hubei 430074, China

[2] China Ship Development and Design Center, Wuhan, Hubei 430064, China

* Corresponding author; E-mail: jianjun_liu@hust.edu.cn

Solution of radiative intensity plays an important role in many areas, such as combustion monitoring, fire detection, and infrared imaging simulation, etc. The reverse Monte Carlo method is a widely used method due to its high accuracy and flexibility. However, it has not been applied to solve radiative intensity in systems discretized by unstructured grids which are usually applied in complex geometries. This brings difficulty if the solution of radiative intensity is applied to practical radiative systems of irregular geometries, especially coupled with other physical problems, such as fluid flow, etc. In this work, the reverse Monte Carlo method based on unstructured grids is developed for solving radiative intensity in participating media with complex geometries. In order to improve the efficiency of ray tracing process, a preprocessing procedure is introduced to establish topological relationships between unstructured grids. Radiative heat flux and radiative intensity in radiative systems with different geometries of a cube and a triangular prism are calculated. Comparing with results of other methods in literatures, radiative heat flux and radiative intensity calculated by the present method shows very good accuracy.

Key words*: Reverse Monte Carlo method; Unstructured grids; Radiative intensity; Complex geometry*

1. Introduction

Solving radiative intensity plays an important role in many engineering applications based on image analysis, such as combustion monitoring of industrial boilers [1, 2], fire detection [3, 4], and infrared imaging simulation[5-7]. Solutions of the Radiative Transfer Equation (RTE) such as the Monte Carlo method [8, 9], the discrete coordinate method [10, 11], the spherical harmonics method [12, 13], and the finite volume method [14] have been proposed and widely used in the past few decades. However, most of these methods are focused on solving the integral radiative quantities such as radiative heat flux. Some of them can solve radiative intensity in limited directions, such as the discrete coordinate method, and the finite volume method. In contrast, in order to analyze radiative images captured by cameras with millions of pixels in real applications, radiative intensities with millions of directions are to be solved, which brings challenge to the above mentioned RTE solutions.

The reverse Monte Carlo (RMC) method is an efficient method for solving directional radiation intensity [15, 16]. Wang et al. [17] performed inverse radiative analysis based on the RMC method, and used the visible radiative images received by the CCD to reconstruct the three-dimensional temperature distribution within the participating medium. Liu et al. [2] reconstructed the temperature distribution of laboratory-scale and large-scale pulverized coal furnaces based on the RMC method. In these applications, the RMC method is used to solve radiative intensity in directions corresponding to the view angles of all the camera pixels. Then, the relationship between the medium emission and the radiative images is established, which is important for temperature reconstruction. Due to the high resolution of the camera and the small field angle of a single pixel, the RMC method is much more efficient than the forward Monte Carlo method for radiative image analysis. The radiative intensity solved by the RMC method has good application prospects in online monitoring of combustion temperature.

Currently, the RMC method are mostly applied to radiative systems with simple geometries which are discretized by structured grids [2, 17]. The ray tracing process is easy to implement. However, in actual applications, the geometries of the computational domain are often irregular and complex. Discretization errors are usually introduced if structured grids are applied to discretize the complex geometry, especially in the zone near the boundaries. Furthermore, most computational fluid dynamics software discretizes the computational domain by unstructured grids, even if the computational domain has simple geometries. It will be convenient if the same set of grids are used to solve the radiative transfer process by the RMC method. Therefore, extending the RMC method to applicable for unstructured grids can not only improve the calculation accuracy of radiative intensity, but also make the radiative transfer computation more convenient to couple with other physical problem such as fluid flow calculation etc.

In this work, the RMC method based on unstructured grids is developed for solving radiative intensity in participating medium with complex geometries. First, the topological relationships between the unstructured grids are established to define their positional relationships. These relationships are helpful for quickly locating the next unstructured grid that the energy bundle will pass through in the ray tracing process. Then, the implementation of the RMC method based on unstructured grids is introduced in detail. Radiative heat flux and radiative intensity with high directional resolution in several geometries are calculated using the present developed method. The results are validated by comparing with those reported in previous studies.

2. Theory

2.1. Fundamental of the reverse Monte Carlo method

For an emitting, absorbing, and scattering gray medium, the radiative transfer equation is expressed as [15]

$$\frac{dI}{ds} = \kappa_a I_b - (\kappa_a + \sigma_s) I + \frac{\sigma_s}{4\pi} \int_{4\pi} I(\hat{s}_i) \Phi(\hat{s}_i, \hat{s})\, d\Omega_i \tag{1}$$

where κ_a is the absorption coefficient, σ_s is the scattering coefficient, and $\Phi(\hat{s}_i, \hat{s})$ is the scattering phase function. Assuming that the participating medium is isotropically scattering, then the integral form of Eq. (1) can be written as

$$I(s) = I(0) e^{-\beta s} + \int_0^s S(s', \hat{s})\, e^{-\beta(s-s')} \beta ds' \tag{2}$$

$$S(s,\hat{s}) = (1-\omega)I_b + \frac{\omega}{4\pi}\int_{4\pi} I(\hat{s}_i)\, d\Omega_i \tag{3}$$

where $\beta = \kappa_a + \sigma_s$, $\omega = \sigma_s/\beta$, and $I(0)$ is the radiative intensity at the boundary.

The RMC method is a numerical method based on statistics principle that solves radiative transfer problems by tracing a large number of energy bundles. To calculate radiative intensity in a specific direction, *N* energy bundles are generated in the considered direction. Once the energy bundles tracing process is finished, *N* different radiative intensity results I_i (i=1, 2, 3, …, *N*) are obtained. Then, the radiative intensity in this direction can be estimated as

$$I = \frac{1}{N}\sum_{i=1}^{N} I_i \tag{4}$$

In order to ensure the accuracy of the results, the calculation error can be evaluated by monitoring the standard deviation. The standard error of the calculated directional radiation intensity I can be expressed as [16, 18]

$$\sigma_I = \frac{1}{N-1}\sqrt{\sum_{i=1}^{N} I_i^2 - \frac{1}{N}(\sum_{i=1}^{N} I_i)^2} \tag{5}$$

Then, the calculation error of the numerical result δ can be evaluated as [18]

$$\delta = \frac{|I - I_{exact}|}{I_{exact}} < 3\frac{\sigma_I}{I} \tag{6}$$

2.2. Implementation of the reverse Monte Carlo method in unstructured grids

Ray tracing process is the most important part to implement the RMC method. In the ray tracing process, the events of absorption, scattering, and reflection of the energy bundles may occur at any location in the medium or at the boundaries. Therefore, it is important to quickly locate the number of the current cell and the next cell the energy bundle will go through. For systems discretized by structured grids, the cell number can be determined easily according to the location coordinates. In contrast, the determination of cell number in unstructured grids is complicated because there is no explicit connection between the cell number and location coordinates. In order to enhance the ray tracing efficiency, a preprocessing algorithm is executed to find out the adjacent cells for each cell.

Take the case that the computational domain is discretized by tetrahedral cells for example, three tetrahedral cells and two triangular cells are shown in Fig. 1. The cells are depicted separately in the sketch in order to show the detail clearly. After grid discretization, the nodes number included in each cell, for example, tetrahedral cell in blue has Nodes A, B, C and D are known, and the coordinates of all the nodes are obtained. However, the position relationships of different cells are unknow. That is to say, for the tetrahedral cell in blue, its adjacent volume cells in green and surface cells in yellow is not known. This brings difficulty to find the next cell that the energy bundle will arrive in ray tracing process. The direct way is traversing all the cells and this leads to high computation cost. In this work, the topological relationships which include the adjacent cells information are established firstly by analyzing the common nodes between different cells. The information is used in the following ray tracing process and make it much more efficient.

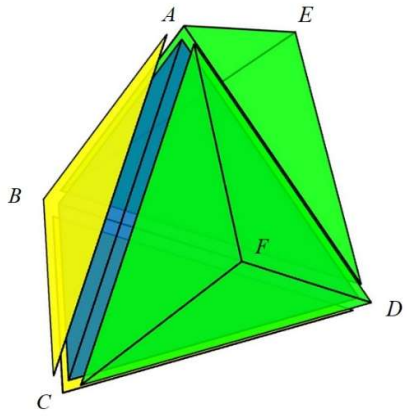

Fig. 1 Topological relationship schematic of unstructured meshes

Once the topological relationships to clarify the positional relationship between unstructured grids are established, the ray tracing process for a single energy bundle can be summarized as follows,

a) Energy bundle emitting. First, the number of the emitting cell is determined based on the coordinates of the emitting point. Then, the emitting direction of the energy bundle is set to be the opposite direction of the radiative intensity to be calculated. The initial energy weight of the bundle w=1, and the initial value of the radiative intensity I_i=0. The optical thickness that the energy bundle will go through in the medium before scattering is determined by

$$O_{ks} = -ln(rand) \tag{7}$$

where O_{ks} is the scattering optical thickness and $rand$ is a random number between 0 and 1 which is generated by the computer.

b) Absorbing and reflecting at boundaries. If the energy bundle reaches a boundary, the energy bundle will be absorbed and reflected by the opaque boundary, or travel through the transparent boundary directly. For a diffuse surface boundary with reflectivity ρ and blackbody radiative intensity $I_{w,b}$, the target radiative intensity in this ray tracing process is updated as,

$$I_i^{new} = I_i + w \cdot (1-\rho) \cdot I_{w,b} \tag{8}$$

Since the energy beam is partially absorbed by the boundary, its remaining energy weight is updated as,

$$w^{new} = w \cdot \rho \tag{9}$$

The remaining energy is reflected by the diffuse boundary, and the polar angle θ and the azimuthal angle ϕ of the reflecting direction can be determined by two random numbers, which are expressed in the local coordinate system as,

$$\theta = sin^{-1}\sqrt{rand} \tag{10}$$

$$\phi = 2\pi \cdot \ rand \tag{11}$$

c) Absorbing or scattering in the medium volume. If the energy bundle travels in a medium volume, the energy bundle will be absorbed and scattered by the participating medium. Assuming the medium volume has absorption coefficient k_a, scattering coefficient k_s, and blackbody radiative intensity I_b, and the geometric length of the ray through the medium volume is s, the target radiative intensity is updated as,

$$I_i^{new} = I_i + w \cdot (1 - e^{-\kappa_a s}) \cdot I_b \tag{12}$$

Due to the absorption of the medium, the remaining energy weight after the energy bundle transmits the medium volume is

$$w^{new} = w \cdot e^{-\kappa_a s} \tag{13}$$

Then, the remaining scattered optical thickness is updated as,

$$O_{ks}^{new} = O_{ks} - \sigma_s s \tag{14}$$

If the scattering optical thickness is reduced to zero, the energy bundle will be scattered by the participating medium. For isotropic scattering medium, the polar angle θ and the azimuthal angle ϕ of the scattering direction can be generated by two random numbers, which are expressed in the local coordinate system as,

$$\theta = sin^{-1}(1 - 2rand) \tag{15}$$

$$\phi = 2\pi \ rand \tag{16}$$

If the remaining energy weight of the tracing bundle is less than a predefined threshold, the tracing process for the current bundle is terminated, and the next energy bundle is processed.

3. Results and discussion

A cube and a triangular prism which have been extensively studied in literatures are employed to test the developed method. Radiative heat flux and directional radiation intensity with high directional resolution are calculated using the developed method. The obtained results are analyzed and compared with those reported in literatures. The present method is implemented by MATLAB programming, and all calculations are completed on a personal computer with an Intel Core i5-8265 processor, and 20 GB RAM. The threshold value of the residual energy bundle is set to be 10^{-6}. In order to limit the impact of statistical uncertainty on calculation accuracy, the value of $3\sigma_I/I$ in Eq. (6) which can be updated in real-time as the number of energy bundles increases is set to be 0.001, which ensures that the biggest error of calculation results is less than 0.1%.

3.1. Radiative transfer in cubic enclosure

A cubic enclosure filled with uniform emitting and scattering medium is shown in Fig. 1. The side length of the cube L is 1.0 m, and all walls are cold and diffuse with a uniform reflectivity ρ. As shown in Fig. 2(a), a cartesian coordinate system originating at the center of the cube is established to describe the distribution of radiative parameters. The cube is discretized by 10033 unstructured volume cells and 1744 unstructured boundary faces, as shown in Fig. 2(b).

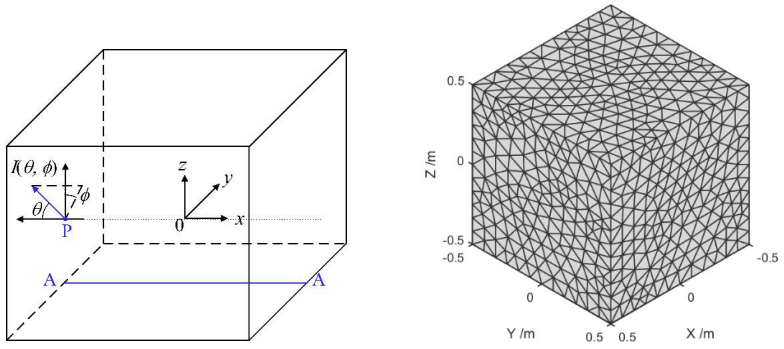

(a) (b)

Fig. 2 The schematic of the cubic enclosure (a) geometry (b) grids

The radiative system considered are the same as that in Ref. [19]. All walls are non-reflective with reflectivity $\rho = 0$. The medium is gray with scattering coefficient $\sigma_s = 0$, and blackbody emissive power E_b. For different absorption coefficients $\kappa_a =$ 0.1, 1.0 and 10.0 m^{-1}, radiative heat flux along line AA as shown in Fig. 1(a), is calculated using the present method. The results are compared with the exact solution provided in Ref. [20] and are shown in Fig. 3. As shown in the figure, the results obtained by the present method are in good agreement with the exact solution.

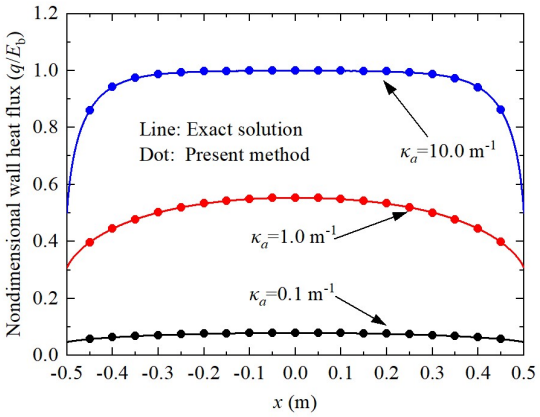

Fig. 3 Comparison of radiative heat flux

In order to verify the reliability of the present method for solving the radiative intensity, the calculating conditions are set to be the same as those in Ref. [16]. The medium within the cube is emitting, absorbing, and isotropically scattering, and is highly heterogeneous in both temperature and optical properties, and the distribution of κ_a, σ_s and E_b is described by Eqs. (17-19). The walls are cold and diffusely reflective. Different cases with wall reflectivity $\rho = 0.0$ and 0.5 are considered. The radiative intensity at point P (-0.5, 0, 0) is calculated.

$$\kappa_a(x,y,z) = \exp\left[-\frac{3(x+0.5L)}{L}\right]\left[1-\sqrt{\frac{2(y^2+z^2)}{L^2}}\right] \tag{17}$$

$$\sigma_s(x,y,z) = \exp\left[-\frac{3(x+0.5L)}{L}\right]\left[1-\sqrt{\frac{2(y^2+z^2)}{L^2}}\right] \tag{18}$$

$$E_b(x,y,z) = E_{b,max}\exp\left[-\frac{3(x+0.5L)}{L}\right]\left[1-\sqrt{\frac{2(y^2+z^2)}{L^2}}\right] \tag{19}$$

The nondimensional radiative intensity $I(\theta,\phi)/(E_{b,max}/\pi)$ in directions with ϕ = 0° and 180° obtained by the present method is presented in Fig. 4. The benchmark solution is provided by the NC-RMC method in Ref. [16], which has been proven to have high accuracy. As shown in the figure, radiative intensity results with wall reflectivity of 0.5 is larger than those with wall reflectivity of 0.0, since the wall reflection keeps more energy stay in the system, which leads to bigger emissive power at the boundary. The results obtained by the present method agree very well with the benchmark solution. It shows that the proposed unstructured RMC method can calculate the radiative intensity with high accuracy.

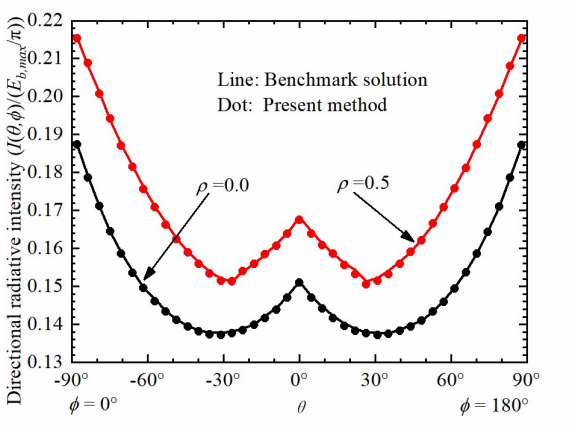

Fig. 4 Comparison of radiative intensity

Radiative intensity with high directional resolution at point P as shown in Fig. 2 is calculated using the present method. An angular discretization using spherical ring with 10 levels is employed and radiative intensities in 265 directions over a semispherical solid angle are obtained. The nondimensional radiative intensities are shown in Fig. 5(a), and the difference comparing with those by the NC-RMC method is shown in Fig. 5(b). As described by Eq. (9), the medium gets hotter at the position closer to point P, so radiative intensity in the direction where its polar angle is close to 90° is greater. This trend is consistent with that presented in the literature. The differences of the results obtained by the present method and those by the NC-RMC method are shown in Fig. 5(b). The biggest difference is less than 0.8%, and the average difference is about 0.2%. This proves that the proposed unstructured reverse Monte Carlo method has high accuracy for solving directional radiation intensity.

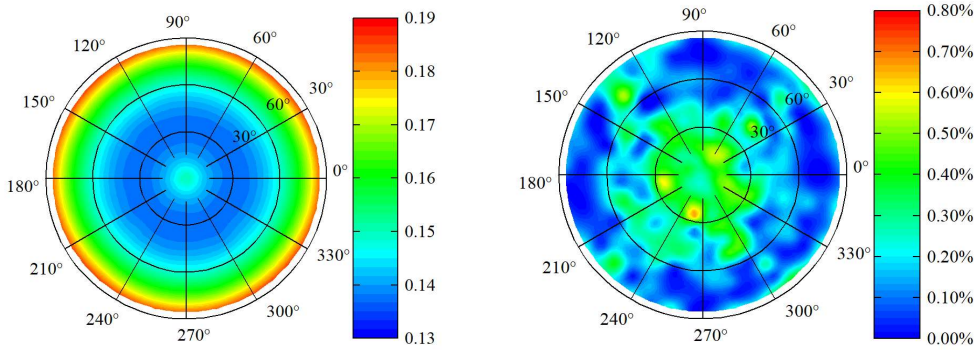

(a) (b)

Fig. 5 Hemispherical radiative intensity at point P (a) nondimensional radiative intensity by the present method (b) radiative intensity difference

3.2. Radiative Transfer in triangular prism enclosure

In this section, a three-dimensional radiative system of equilateral triangular prism as shown in Fig. 6(a) which has been investigated in Ref. [21] is considered. The three-dimensional equilateral triangular prism is filled with absorbing and emitting media assigned uniform emissive power. The walls are cold and black. The size parameters L and H as labelled in Fig. 6(a) are all equal to 1.0 m. The computational domain is discretized by 1615 unstructured grids, as sketched in Fig. 5(b). The unstructured grids employed in this system are not as fine as those shown in Fig. 2(b).

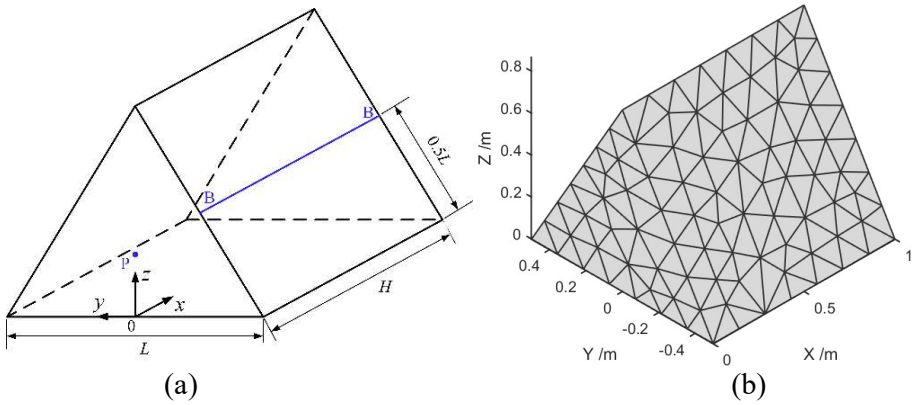

(a) (b)

Fig. 6 The schematic of the triangular prism enclosure (a) geometry (b) grids

For different absorption coefficients κ_a= 0.1, 1.0 and 10 m^{-1}, the results of radiative heat flux along the BB line, the blue line as shown in Fig. 6(a), are calculated and shown in Fig. 7. The benchmark results provided in Ref. [21] are also shown in the figure. Results by these two methods confirm very well with each other. The biggest difference is less than 0.2%. It is worth noting that for the uniform medium considered in this figure, grid discretization does not introduce additional errors. The calculation errors of the present method are all introduced by statistical property of the Monte Carlo method. Then, even if the unstructured grid in Fig. 6(b) is coarse, the present method can obtain radiative heat flux with high accuracy.

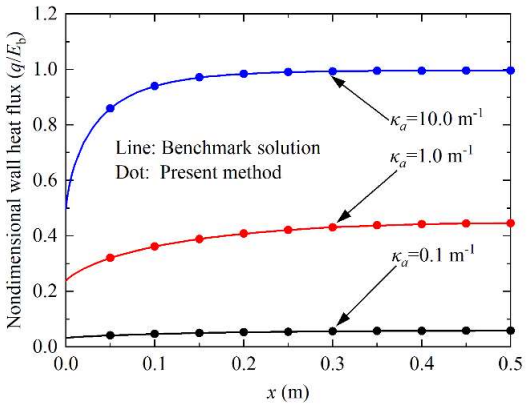

Fig. 7 Comparison of radiative heat flux

In order to investigate the accuracy of the radiative intensity calculated by the unstructured RMC method, radiative intensity at the center point of the x = 0 plane, as indicated by point P in Fig. 6(a) is calculated by both the unstructured RMC method developed in the current work and the NC-RMC method in Ref. [16]. The system is discretized by 1615 unstructured grids, which are the same as those in Fig. 6. The triangular prism is filled with absorbing, emitting and isotropically scattering medium, and non-uniform medium with absorption coefficient, scattering coefficient, and emissive power described in Eqs. (20-22) is considered. The walls are cold and black. The spherical ring angle set with 20 levels, which corresponds to 1029 discrete directions in hemisphere, is used for angle discretization.

$$\kappa_a(x,y,z) = 5\exp\left(-\frac{3x}{L}\right)\left[1-\sqrt{\frac{3\left[y^2+\left(z-\sqrt{3}L/6\right)^2\right]}{L^2}}\right] \tag{20}$$

$$\sigma_s(x,y,z) = 5\exp\left(-\frac{3x}{L}\right)\left[1-\sqrt{\frac{3\left[y^2+\left(z-\sqrt{3}L/6\right)^2\right]}{L^2}}\right] \tag{21}$$

$$E_b(x,y,z) = E_{b,max}\exp\left(-\frac{3x}{L}\right)\left[1-\sqrt{\frac{3\left[y^2+\left(z-\sqrt{3}L/6\right)^2\right]}{L^2}}\right] \tag{22}$$

Nondimensional radiative intensity $I(\theta,\phi)/(E_{b,max}/\pi)$ calculated by the unstructured RMC method is presented in Fig. 8 (a). In the triangular prism, since the optical thickness varies in different directions, the radiative intensity distribution shows a similar triangle in the center of the figure. The difference between the results obtained by the present method and the benchmark solution is shown in Fig. 8(b). The largest difference is 3.1%, and the average difference is larger than 0.8%. Besides, the differences in 55 directions are greater than 2.0%. Most of the directions with large errors are those with a polar angle close to 90°. This is because the grid discretization here is coarse, and the current grid set cannot accurately describe the large varying gradient of the radiative parameters in the non-uniform medium close to point P.

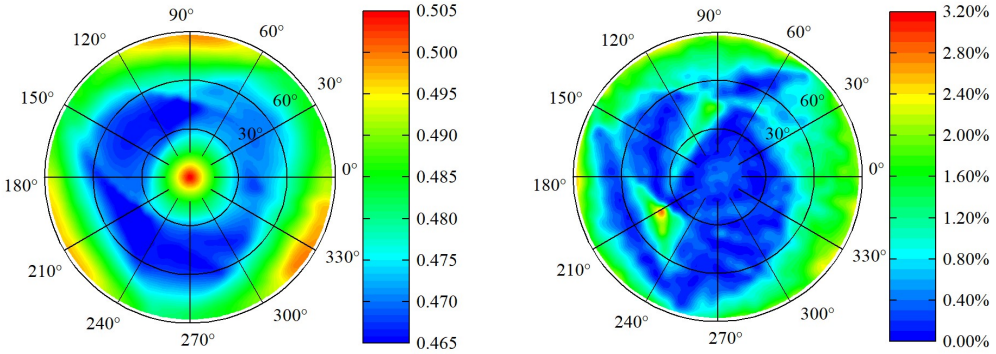

(a) (b)

Fig. 8 Hemispherical radiative intensity at point P with 1615 unstructured grids (a) nondimensional radiative intensity by the present method (b) radiative intensity difference

In order to improve the calculation accuracy of the present method, a refined grid set with 27150 unstructured grids as shown in Fig. 9 is applied. Fig. 10 shows the nondimensional radiation intensity calculated by the present method, and the difference compared with the benchmark solution. As shown in Fig. 10(a), the triangle shape in the intensity figure has more obvious symmetrical feature, which shown higher accuracy of radiative intensity results compared with those in Fig. 8(a). Furthermore, the biggest difference compared with the benchmark solution is less than 1.0%, and the average difference is about 0.3%. In this case, the medium has strongly heterogeneous optical properties, and the calculation accuracy of the unstructured RMC method is significantly improved by refining the unstructured grids.

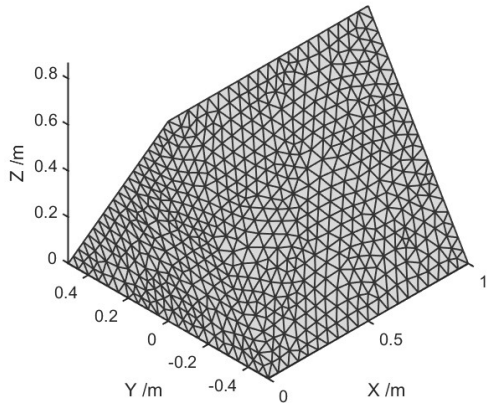

Fig. 9 The refined unstructured grids

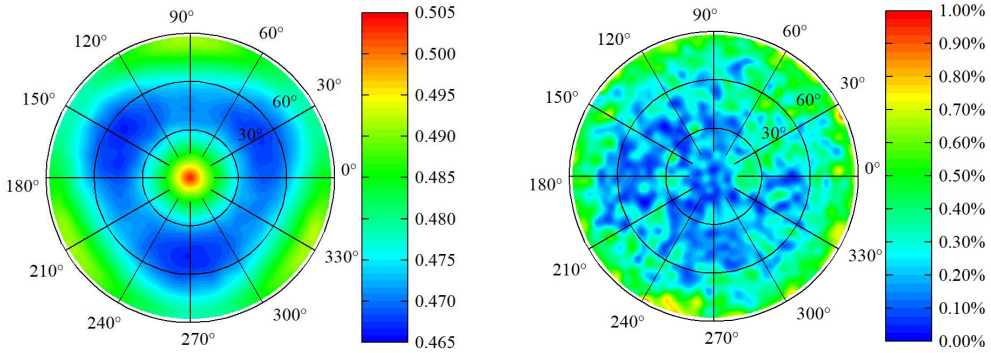

(a) (b)

Fig. 10 Hemispherical radiative intensity at point P with 27150 unstructured grids (a) nondimensional radiative intensity by the present method (b) radiative intensity difference

4. Conclusion

In this paper, a reverse Monte Carlo method based on unstructured grids is developed for solving radiative intensity in participating medium with complex geometries. Two radiative systems with cube and triangular prism enclosures containing emitting, absorbing, non-scattering and scattering, uniform and non-uniform participating media are employed to test the present developed method. Both radiative heat flux and directional radiation intensity with high directional resolution are calculated by the present method and compared with those reported in literatures. The results of the present method have very good agreement with those of benchmark solutions. In all considered cases, the biggest differences of radiative intensity in hundreds or thousands of directions are all less than 1.0%, and the average differences are all less than 0.3%. The present study shows that the developed method adapts well to a variety of complex geometries and is suitable for unstructured grids, which brings huge advantages to solve practical problems, especially combined with other physical problems such as fluid flow.

Nomenclature

E emissive power, [Wm^{-2}]

I radiative intensity, [$Wm^{-2}sr^{-1}$]

κ_a absorption coefficient, [m^{-1}]
σ_s scattering coefficient, [m^{-1}]
O optical thickness, [–]
rand random number, [–]
s geometry path length, [m]
$\hat{s}$ unit vector into a given direction, [–]
S radiative source function, [$Wm^{-2}sr^{-1}$]
w weight of energy bundles, [–]
β extinction coefficient, [m^{-1}]
δ calculation error, [–]
θ polar angle, [°]
ρ reflectivity, [–]
σ standard error, [–]
ϕ azimuthal angle, [°]
Φ scattering phase function, [sr^{-1}]
ω scattering albedo, [–]
Ω solid angle, [sr]

subscripts

b blackbody value
i incoming direction
w wall value

References

[1] Zhou, H.-C., *et al.*, Experimental investigations on visualization of three-dimensional temperature distributions in a large-scale pulverized-coal-fired boiler furnace, *Proceedings of the Combustion Institute*, *30*. (2005), 1, pp. 1699-1706

[2] Liu, D., *et al.*, Experimental reconstructions of flame temperature distributions in laboratory-scale and large-scale pulverized-coal fired furnaces by inverse radiation analysis, *Fuel*, *93*. (2012), pp. 397-403, DOI No. 10.1016/j.fuel.2011.09.004

[3] Calle, A., *et al.*, Fire detection and monitoring using MSG Spinning Enhanced Visible and Infrared Imager (SEVIRI) data, *Journal of Geophysical Research: Biogeosciences*, *111*. (2006), G4, DOI No. https://doi.org/10.1029/2005JG000116

[4] Bordbar, H., *et al.*, Flame detection by heat from the infrared spectrum: Optimization and sensitivity analysis, *Fire Safety Journal*, *133*. (2022), p. 103673, DOI No. https://doi.org/10.1016/j.firesaf.2022.103673

[5] Zhou, Y., *et al.*, A numerical simulation method for aircraft infrared imaging, *Infrared Physics & Technology*, *83*. (2017), pp. 68-77, DOI No. https://doi.org/10.1016/j.infrared.2017.04.011

[6] Mo, D., *et al.*, Similarity criteria of target thermal radiation characteristics and their application to infrared radiation of jet engine exhaust system, *International Journal of Thermal Sciences*, *125*. (2018), pp. 358-368, DOI No. https://doi.org/10.1016/j.ijthermalsci.2017.12.003

[7] Huang, K.,X. Mao, Detectability of infrared small targets, *Infrared Physics & Technology*, *53*. (2010), 3, pp. 208-217, DOI No. https://doi.org/10.1016/j.infrared.2009.12.001

[8] Walters, D.V.,R.O. Buckius, Monte Carlo methods for radiative heat transfer in scattering media, *Annual Review of Heat Transfer*, *5*. (1994), pp. 131-176

[9] Farmer, J.T.,J.R. Howell, Monte Carlo prediction of radiative heat transfer in inhomogeneous, anisotropic, nongray media, *Journal of Thermophysics and Heat Transfer*, *8*. (1994), 1, pp. 133-139

[10] Fiveland, W.A., Discrete-Ordinates Solutions of the Radiative Transport Equation for Rectangular Enclosures, *Journal of Heat Transfer*, *106*. (1984), 4, pp. 699-706

[11] Truelove, J.S., Three-dimensional radiation in absorbing-emitting-scattering media using the discrete-ordinates approximation, *Journal of Quantitative Spectroscopy and Radiative Transfer*, *39*. (1988), 1, pp. 27-31, DOI No. 10.1016/0022-4073(88)90016-7

[12] Cheng, P., Dynamics of a radiating gas with application to flow over a wavy wall, *AIAA Journal*, *4*. (1966), 2, pp. 238-245, DOI No. 10.2514/3.3424

[13] Mengüç, M.P.,R. Viskanta, Radiative transfer in three-dimensional rectangular enclosures containing inhomogeneous, anisotropically scattering media, *Journal of Quantitative Spectroscopy and Radiative Transfer*, *33*. (1985), 6, pp. 533-549, DOI No. https://doi.org/10.1016/0022-4073(85)90021-4

[14] Raithby, G.D.,E.H. Chui, A Finite-Volume Method for Predicting a Radiant Heat Transfer in Enclosures With Participating Media, *Journal of Heat Transfer*, *112*. (1990), 2, pp. 415-423

[15] Modest, M.F.,S. Mazumder, *Radiative Heat Transfer*. Academic Press, 2022.

[16] Cheng, Y., *et al.*, Solution of radiative intensity with high directional resolution in heterogeneous participating media and irregular geometries by the null-collision reverse Monte Carlo method, *International Journal of Heat and Mass Transfer*, *152*. (2020), p. 119475, DOI No. https://doi.org/10.1016/j.ijheatmasstransfer.2020.119475

[17] Wang, F., *et al.*, Efficient inverse radiation analysis of temperature distribution in participating medium based on backward Monte Carlo method, *Journal of Quantitative Spectroscopy and Radiative Transfer*, *109*. (2008), 12-13, pp. 2171-2181, DOI No. 10.1016/j.jqsrt.2008.03.002

[18] Kalos, M.H.,P.A. Whitlock, *Monte Carlo Methods*. Wiley, 2008.

[19] Fan, C., *et al.*, An unstructured Monte Carlo ray-tracing method for solving radiative heat transfer in 3D gray semitransparent medium, *Journal of Quantitative Spectroscopy and Radiative Transfer*, *225*. (2019), pp. 110-118, DOI No. https://doi.org/10.1016/j.jqsrt.2018.12.035

[20] Sakami, M., *et al.*, Radiative heat transfer in three-dimensional enclosures of complex geometry by using the discrete-ordinates method, *Journal of Quantitative Spectroscopy and Radiative Transfer*, *59*. (1998), 1, pp. 117-136, DOI No. https://doi.org/10.1016/S0022-4073(97)00023-X

[21] Grissa, H., *et al.*, Prediction of radiative heat transfer in 3D complex geometries using the unstructured control volume finite element method, *Journal of Quantitative Spectroscopy and Radiative Transfer*, *111*. (2010), 1, pp. 144-154, DOI No. https://doi.org/10.1016/j.jqsrt.2009.07.006

Submitted: 27.12.2024.
Revised: 24.02.2025.
Accepted: 26.02.2025.